NRC·CNRC

NRC Publications Archive
Archives des publications du CNRC

Investigation of numerical modelling techniques for predicting highly nonlinear extreme waves in shallow and deep water

Islam, Mohammed; Zaman, Hasanat; Jahra, Fatima

This publication could be one of several versions: author's original, accepted manuscript or the publisher's version. / La version de cette publication peut être l'une des suivantes : la version prépublication de l'auteur, la version acceptée du manuscrit ou la version de l'éditeur.
For the publisher's version, please access the DOI link below./ Pour consulter la version de l'éditeur, utilisez le lien DOI ci-dessous.

Publisher's version / Version de l'éditeur:
https://doi.org/10.23919/OCEANS44145.2021.9705943
OCEANS 2021 (San Diego – Porto), 2022-02-15

NRC Publications Archive Record / Notice des Archives des publications du CNRC :
https://nrc-publications.canada.ca/eng/view/object/?id=07e3f2cf-c558-4e4a-9e03-bdd72517013d
https://publications-cnrc.canada.ca/fra/voir/objet/?id=07e3f2cf-c558-4e4a-9e03-bdd72517013d

Access and use of this website and the material on it are subject to the Terms and Conditions set forth at
https://nrc-publications.canada.ca/eng/copyright
READ THESE TERMS AND CONDITIONS CAREFULLY BEFORE USING THIS WEBSITE.

L'accès à ce site Web et l'utilisation de son contenu sont assujettis aux conditions présentées dans le site
https://publications-cnrc.canada.ca/fra/droits
LISEZ CES CONDITIONS ATTENTIVEMENT AVANT D'UTILISER CE SITE WEB.

Questions? Contact the NRC Publications Archive team at PublicationsArchive-ArchivesPublications@nrc-cnrc.gc.ca. If you wish to email the authors directly, please see the first page of the publication for their contact information.

Vous avez des questions? Nous pouvons vous aider. Pour communiquer directement avec un auteur, consultez la première page de la revue dans laquelle son article a été publié afin de trouver ses coordonnées. Si vous n'arrivez pas à les repérer, communiquez avec nous à PublicationsArchive-ArchivesPublications@nrc-cnrc.gc.ca.

National Research Council Canada | Conseil national de recherches Canada

Canada

Investigation of Numerical Modelling Techniques for Predicting Highly Nonlinear Extreme Waves in Shallow and Deep Water

Mohammed Islam
Ocean, Coastal and River Engineering Research Center
National Research Council Canada
St. John's, NL Canada
Mohammed.Islam@nrc-cnrc.gc.ca

Hasanat Zaman
Ocean, Coastal and River Engineering Research Center
National Research Council Canada
St. John's, NL Canada
Hasanat.Zaman @nrc-cnrc.gc.ca

Fatima Jahra
Fleetway Inc.
St. John's, NL Canada
jahra.fatima@fleetway.ca

***Abstract*—This paper aims to investigate the accuracy and computational efficiency of three CFD-based numerical codes to accurately simulate extremely large regular and irregular waves of different steepness in deep and shallow water conditions. The work assesses the performance of three numerical techniques with different formulations of the fluid dynamic equations. Firstly, an open-sourced smoothed particle hydrodynamics (SPH) code; secondly, a finite difference method (FDM) based 3D numerical model with the assumption of inviscid and incompressible fluid flow; and thirdly, a commercial CFD code that uses a finite volume method (FVM) to solve the Reynolds-averaged Navier-Stokes (RANS) equations. A suite of metrics and methodologies, considering three key performance parameters: accuracy, computational requirements and available features for providing a consistent framework for the quantitative assessment of different techniques, has been presented. Numerically simulated free surface elevations, wave periods, and spectrum (for irregular waves only) are compared with experimental data previously acquired at an Offshore Engineering Basin (OEB) facility. Extensive convergence studies were carried out for each numerical tool for a selected large wave before predictions were model for all waves. All three models reproduced waves with an accuracy comparable to physical wave makers in the wave basin experiments for the deep-water regular and irregular waves; however, the SPH model performed better than the other two models for the shallow water waves. The challenge remains for wave basins to reduce unwanted basin effects and numerical facilities to accurately model waves with proper account for boundary effects and numerical diffusions. In addition, only flat-bottom domains were considered in the investigation, leaving the wave modelling for uneven bottom for future studies.**

Keywords—Nonlinear Extreme waves, numerical modelling, physical experiments, SPH, predictions comparisons.

I. Introduction

As a conventional practice, the design of any floating or fixed marine structure located in the coastal or offshore regions is evaluated by performing scaled model testing in a wave basin under simulated real-sea conditions to study the fluid-structure interactions involved and subsequently, to refine the design. Depending on the complexity of the setup and evaluation requirements, this process can be costly and time-consuming. However, due to the increase of computational power and advancement of nonlinear numerical modelling of ocean waves in recent years, computational fluid dynamics (CFD)-based numerical wave tanks (NWTs) are increasingly being used as a supplementary tool to physical modelling, which is generally inexpensive, efficient and relatively quick. That is, provided that the numerical model can reproduce the real-life environment and the underlying physical processes.

From the viewpoint of water depths and wavelengths relationship, the ocean waves, in general, are of two major categories, deep water waves and shallow-water waves. As per the definition, a deep water wave is not agitated by the sea bottom effects and is defined as the wave propagating over a water depth larger than half of its wavelength. This kind of wave propagates far away without any significant changes in its waveform until it breaks. A detailed description of the basic theory might be found in [37] or [38] or other similar literature.

On the other hand, a shallow water wave has a wavelength more than double the local water depth, and consequently, this type of wave is highly influenced by the sea bottom depending on the local water depth to wavelength ratio known as relative water depth. Thus, the relative water depth index defines the shallowness of the propagating wave. A cut-off point of relative water depth is equal to or greater than 0.5 defines the deep-water wave condition. In contrast, this parameter smaller than 0.5 outlines the shallow water wave, and a lower value of relative water depth intensifies the shallowness. Under some conditions, the shallow water wave is also known as a long wave and inherits considerable non-linearity that forces the wave to undergo many changes in its original form and characteristics. A proper balance in non-linearity and the dispersion relation can help such waves to propagate long distances without much change in their form. The characteristics of such waves are well described in much literature. [39], [40], [41], [42], [43] are few to mention here.

The accuracy of an NWT is driven by the underlying numerical modelling approach, which is often simplified to reduce the computational burden. Three primary methods targets to solve the Laplace equations, Euler equations and

Copyright © 2021 by National Research Council Canada

Navier Stokes equations. Depending on which equations are solved, the numerical techniques are termed differently: the potential flow-based boundary element method (BEM), finite difference method (FDM), the finite volume method (FVM), the finite element method (FEM), and Smoothed Particle Hydrodynamics (SPH) method, to name a few. Low fidelity models, e.g., potential flow-based NWTs, implementing the Laplace equation, can compute results with minimal computational cost and are valuable for parametric studies. However, due to the underlying assumptions of inviscid fluid and small amplitude wave and body motion, the range over which these models are valid is often exceeded for offshore and marine engineering applications. Compared to lower fidelity numerical tools, high-fidelity numerical models, such as CFD (FVM, FEM and SPH)-based NWTs have the advantage of capturing relevant hydrodynamic non-linearities, such as complex free surface elevation (including wave breaking), viscous drag and turbulence effects. Although these methods are more computationally costly than their lower fidelity counterparts, they can deliver accurate results in high resolution, which is particularly useful for investigating specific flow phenomena around coastal and offshore structures. In particular, CFD-based methods implementing the Reynolds Averaged Navier–Stokes (RANS) equations are becoming more common in coastal and offshore engineering due to the increasing availability and decreasing the cost of high-performance computing power [35].

The RANS-based models are also known as the phase-averaged models used to study waves with principally random phases. For example, see [44] and others and also there is Reynolds Averaged Navier Stokes (RANS) model see [45]. For vertically integrated type models, see [46], for example. On the other hand, the phase-resolving models are extensively adopted to study the nonlinear shallow-water effects. Moreover, the phase-resolved modelling of the far-field is essential for providing a realistic wave boundary condition for near-field CFD wave modelling. For detail, refer to [47] or others concerning Boussinesq type models, and for boundary value problems, see [48].

Some models are exclusively for deep or shallow water waves, and some are for deep-shallow water waves [4]. All of the models stated above have different advantages and disadvantages regardless of whether numerical methods or schemes are used. Adopting a suitable numerical model depends on many factors; some are the purpose to be served, accuracy needed, available computational power and simulation time. There is enormous literature in this field containing various information about wave generation, propagation, and decay for different conditions. But still, a lot more information is required to be known to update our present understanding in this field. Researchers are starving for more efficient tools to study different flow characteristics in the Ocean.

Previously, different wave models are developed by different developers and institutes, often with various numerical implementations, making a direct comparison among the modelling techniques difficult. A noteworthy initiative is the REEF3D [36], developed into an open-source hydrodynamic numerical toolbox that consists of several modules based on the Navier–Stokes equations, the shallow water equations and the fully nonlinear potential theory. This appears to be a good tool that incorporates the majority of the grid-based techniques discussed above. Windt et al. (2019) [34] applied several numerical wave makers (NWMs) available in the open-source CFD software, OpenFOAM. The authors found the NWTs capable of reproducing waves with an accuracy comparable to real wave makers in physical wave tank experiments. However, the authors showed that significant differences are found between the various NWTs, and no single method performed best in all aspects of the assessment across the different test cases.

Among the grid-less methods, the particle method has advantages in handling nonlinear free-surface flows and complicated interactions with fixed/floating bodies. One of the well-developed particle methods is smoothed particle hydrodynamics (SPH) that was originally developed for astrophysics, and it was first applied to free-surface flow problems by Monaghan [24]. Since SPH is a mesh-less and Lagrangian method, special treatment is not required to track the free surface, while a lot of numerical difficulties and problems need to be solved in mesh-based CFDs. Although the traditional grid-based numerical methods, in some circumstances, are better-developed methods than the SPH method, they have difficulties in handling some complex phenomena such as nonlinear shallow-water waves. This motivated researchers to seek alternatives to solve these problems, and the SPH method has become a good choice.

This paper investigates the accuracy and computational efficiency of three CFD-based numerical codes, with a particular focus on an SPH-based code to simulate accurately moderate to huge regular and irregular real-world waves of different steepness in both deep water and shallow water conditions. An SPH-based two-dimensional numerical wave tank (NWT) is used for numerical simulation and is accelerated by a graphical processing unit (GPU), assuming future applications to realistic engineering problems. A commercial RANS-solver-based wave model and an in-house developed FDM- and Eulerian-based wave model are also used for the same waves for the comparative study. In addition, CFD predictions of irregular waves and subsequently, FFT analysis is carried out, and the resulting wave spectrum is compared with the basin measured wave spectrum and the relevant theoretical spectrum. Through these validation and comparison studies, a detailed discussion on the accuracy of SPH, RANS and Eulerian simulation of water waves is made and provides a recommended set of numerical parameters. The motivation is to develop and enhance numerical tools to complement physical wave basins for studying marine, and coastal structures in harsh environments and, in the way, raise the expectation bar from the wave basin. Section 2 provides a brief account of the offshore basin used for measuring the waves under investigation. Section 3 presents the details of the three numerical models and setup descriptions of the NWTs. Section 4 presents the results of the convergence studies and detailed comparisons between the numerical model predictions and corresponding measurements. A few concluding remarks and recommendations for future works follow.

 Copyright © 2021 by National Research Council Canada

II. PHYSICAL MODELING

The Offshore Engineering Basin (OEB) of the National Research Council Canada's Ocean Coastal and River Engineering Research Centre (the NRC-OCRE) was utilized to conduct an extensive test program to model several regular and irregular shallow and deep water waves. In this paper, we present a sub-set of the wave data that are used to compare with the numerical model predictions. Table 1 presents the test matrix of the wave characteristics and wave types modelled in the present research.

TABLE 1. THE SIMULATION MATRIX FOR EVALUATING SHALLOW AND DEEP WATER AND REGULAR AND IRREGULAR WAVES

ID	Water Depth (h, m)	Height, H/Hs (m)	Period T/Tp (s)	Wave length, L (m)	(h/L)	Steepness (H/L)	Wave Type	Wave Shape	Basin Scale
1	30.3	6.0	8.61	148.4	0.2041	0.0404	Inter	Regular	60
2	30.3	6.0	12.91	222.6	0.1361	0.0270	Inter-Shallow	Regular	60
3	30.3	6.0	25.82	445.1	0.0681	0.0135	Shallow	Regular	60
4	30.3	6.0	11.00	189.6	0.1598	0.0316	Inter-Shallow	Irregular	60
5	126.0	22.0	20.10	560.1	0.2250	0.0393	Inter	Irregular	45

The NRC-OCRE's Offshore Engineering Basin (OEB) is 75m long, 32m wide, and can accommodate water depths up to 3.2 m. The typical water depth for offshore testing is 2.8 m. Waves are generated by 168 independently controlled segmented wave generators, arranged in an L-configuration, producing a multi-directional wave with large spreading angles (-60 degrees to 150 degrees) depending on wave height and period. Each segmented wave generator is 2 m high and 0.5 m wide and can be adjusted vertically to suit different water depths. The segmented generators can operate in five different articulation modes – flapper, piston, and three combinations of flapper and piston modes, optimizing wave quality in deep, shallow, and intermediate water depths, respectively. Passive wave absorption was accomplished by using expanded metal sheets with varying porosity and spacing. This absorber type has excellent absorption characteristics. Fig. 1 shows the OEB layout.

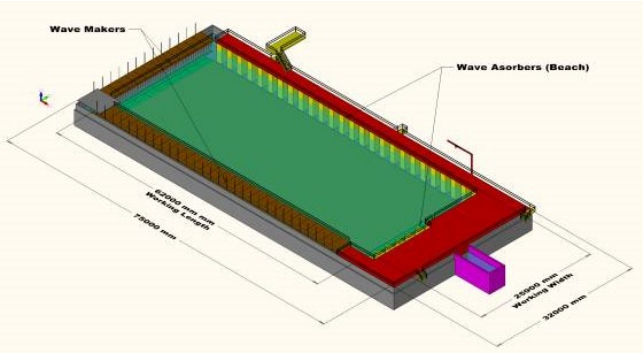

Fig. 1. The NRC-OCRE's Offshore Engineering Basin (OEB) Layout.

The NRC-OCRE's OEB can produce long and short crested waves with a significant height of up to 0.5 m (model scale). Wave reflections from the expanded metal beaches are typically 3-5% depending on wavelength. Wind modelling can be provided via all industry-standard wind spectrums, and current can be provided with a speed of 0.14 m/s at full depth and higher speeds in shallow water depths. Random waves can be generated using the Random Phase and the Random Fourier Coefficient methods. The facility can generate short-crested waves using single- and double-summation methods. Wave direction can be varied from 0˚ to 90˚.

We have presented three regular waves and two irregular waves for this research program, see Table 1. At least 100 cycles of each regular wave are recorded to ensure accurate measurements of wave characteristics and basin reflection measures. In addition, two irregular long-crested wave conditions based on a JONSWAP spectrum (shallow water wave) and Torsethaugen spectrum (transitional water wave) with a peak enhancement (γ) of 2.0 and 3.3, respectively, are also presented. The irregular waves are generated for a 3-hour full-scale duration. All waves were calibrated without wind and current.

III. NUMERICAL MODELING

The work assesses the performance of three numerical models with different formulations of the fluid dynamic equations. Firstly, an open-sourced SPH code is used, a grid-less Lagrangian approach capable of achieving good accuracy in tracking large deformations of a free surface. Secondly, a 3D numerical model with the assumption of inviscid and incompressible fluid flow to evaluate wave kinematics is used. Thirdly, a commercial CFD code is used, a finite volume method that solves the Reynolds-averaged Navier-Stokes (RANS) equations with a volume of fluid (VOF) technique for the free surface tracking, which also accounts for turbulence and viscosity. A brief description of each numerical model, including the NWTs and setup conditions, is presented in the following sub-sections.

A. Smooth Particle Hydrodynamics (SPH) Method

SPH currently represents one of the most popular meshless Lagrangian particle models (e.g., Violeau and Rogers, 2016) [1]. Over the course of recent decades, the SPH has been applied to a broad range of flow processes and fluid-structure interaction problems like sloshing phenomena [8], water entry of solid bodies [9], flow impacts [10], environmental problems [11], free-surface open channels [12] and jets into water bodies [13]. In the field of offshore and coastal engineering, SPH, for example, applied to investigate wave propagation [14] and wave generation and absorption [15] processes, and the interaction of regular or irregular waves with structures such as vertical [16], perforated [17] and porous [18] breakwaters, floating objects [19] and wave energy devices [20] and [21].

DualSPHysics is an open-sourced numerical tool based on the Smoothed Particle Hydrodynamics (SPH) method. A complete description of DualSPHysics can be found in [22]. DualSPHysics follow the fundamentals of SPH, which is a Lagrangian and mesh-less method where the fluid is discretized into a set of particles that are nodal points where physical quantities (such as position, velocity, density, pressure) are computed as an interpolation of the values of the neighbouring particles. The contribution of these neighbours is weighted using a kernel function (W) that measures that contribution starting from the initial particle spacing. This distance between particles is normalized using the smoothing length (h), which is

Copyright © 2021 by National Research Council Canada

the characteristic length that defines the area of influence of the kernel. The kernel presents compact support so that the contribution of particles beyond a cut-off distance (here 2h) is not considered. The remainder of this section presents a brief description of SPH basics and the governing equations and boundary conditions implemented in DualSPHysics.

a) SPH Basics

The mathematical fundamentals of SPH are based on integral interpolants. SPH is an interpolation method whereby any function can be expressed using the values of the different properties (velocity, density, pressure) of a set of particles. The basic principle of SPH is to approximate any function F (r) by the discrete integral interpolants using the smoothing kernel function W (r, h) as follows:

$$F(r_a) \approx \sum_b F(r_b)\frac{\rho_b}{m_b}W(r_a - r_b, h) \tag{1}$$

where $\boldsymbol{\rho}_b$ and m_b are density and mass, respectively, r_a-r_b is the distance between particles, and h determines the maximum distance between interacting particles. The summation is calculated over all the particles b within the region where the kernel is defined. The performance of an SPH model depends heavily on the choice of the smoothing kernel. Kernels are expressed as a function of the non-dimensional distance between particles (q), given by q=r/h, where r is the distance between any two given particles a and b, and the parameter h (the smoothing length) controls the size of the area around particle a in which neighbouring particles are considered. Within DualSPHysics, the Quintic [Wendlend, 1995] [23] kernel from the Wendland kernel family is often recommended:

$$W(r,h) = \alpha_D\left(1 - \frac{q}{w}\right)^4(2q+1) \qquad 0 \le q \le 2 \tag{2}$$

where, $q = (r_a - r_b)/h$, αD is equal to $7/4\pi h^2$ in 2D and $21/16\pi h^3$ in 3D. Following the definition of q, the smoothing radius is 2h.

b) Governing Equations

The mass and momentum conservation laws (Navier-Stokes equations) that govern the dynamics of fluid motion are given in Lagrangian form by:

$$\begin{aligned}\frac{D_\rho}{D_t} &= -\rho\nabla\cdot\boldsymbol{v}\\ \frac{D_v}{D_t} &= -\frac{1}{\rho}\nabla \mathrm{p} + \nu\nabla^2\boldsymbol{v} + g\end{aligned} \tag{3}$$

where v is the velocity, t is the time, p is the pressure, is the ν is the kinematic viscosity, and g is the gravity. In DualSPHysics, the SPH formulation of the above two equations treats the fluid as weakly compressible, and Tait's equation of state is used to couple the two equations to determine fluid pressure based on particle density (Monaghan, 1994) [24]. Following (Monaghan et al., 1999) [25], the relationship between pressure and density follows the expression:

$$p = \frac{\rho_0 c_0^2}{\gamma}\left[\left(\frac{\rho}{\rho_0}\right)^\gamma - 1\right] \tag{4}$$

where ρ_0 is the reference density, $c_0 = c(\rho_0) = \sqrt{(\partial p/\partial\rho)\big|_{\rho_0}}$ is the speed of sound at reference density 0 = 1000 kg/m3, p is the pressure, and γ is an empirical constant that depends on the fluid (e.g. $\gamma = 7$ for water). The compressibility is adjusted so that the speed of sound can be artificially lowered; this means that the size of time step taken at any one moment (which is determined according to a Courant condition, based on the currently calculated speed of sound for all particles) can be maintained at a reasonable value. Such adjustment, however, restricts the sound speed to be at least ten times faster than the maximum fluid velocity, keeping density variations to within less than 1%, and therefore not introducing major deviations from an incompressible approach.

Employing the standard SPH interpolation approximation (Mohaghan, 2012 [26] and Liu and Liu, 2010 [27]) to discretize the conservations equations and incorporating the laminar viscous stresses and Sub-Particle Scale (SPS) to represent the effects of turbulence lead to the SPH forms of the Navier-stokes equations:

$$\begin{aligned}\frac{D_{\rho_a}}{D_t} &= \sum_b m_b(v_a - v_b)\cdot\nabla_a \mathrm{W}_{ab}\\ &\quad + 2\delta h c_0\sum_b m_b\left(\frac{\rho_a}{\rho_b} - 1\right)\frac{r_{ab}}{r_{ab}^2 + \eta^2}\\ &\quad \cdot\nabla_a W_{ab}\end{aligned} \tag{5}$$

$$\begin{aligned}\frac{D_{v_a}}{D_t} &= -\sum_b m_b\left(\frac{p_a}{\rho_a^2} + \frac{p_b}{\rho_b^2}\right)\nabla_a \mathrm{W}_{ab}\\ &\quad + \sum_b m_b\left(\frac{4\nu\boldsymbol{r}_{ab}\cdot\nabla_a W_{ab}}{(\rho_a + \rho_b)(r_{ab}^2 + \eta^2)}\right)\mathbf{v}_{ab}\\ &\quad + \sum_b m_b\left(\frac{\tau_a}{\rho_a^2} + \frac{\tau_b}{\rho_b^2}\right)\nabla_a \mathrm{W}_{ab} + g\end{aligned} \tag{6}$$

where $r_{ab} = |\boldsymbol{r}_{ab}|, \boldsymbol{r}_{ab} = r_a - r_b, \boldsymbol{v}_{ab} = v_a - v_b$ and $\nabla_a W_{ab} = \nabla_a W(r_a - r_b, \mathrm{h})$. The second term on the right-hand side of Equation 4 is the delta-SPH (Molteni and Colagrossi, 2009) [28], which is diffusive and helps to reduce the numerical noise from the density fluctuations and to stabilize the pressure field. δ is a free parameter that needs to be attributed to a suitable value. However, $\delta = 0.1$ is recommended in DualSPHysics and works well for most applications (Crespo et al., 2015) [22]. The second term on the right-hand side of Equation 5 is the discrete form of the viscous stress (Lo and Shao, 2009 [29]), whereas the third term is the sub-particle scale (SPS) term, where τ is the SPS stress tensor (Dalrymple and Rogers, 2006) [14]. DualSPHysics also offers the artificial viscosity scheme proposed by Monaghan (1992) [30], which is a common method within fluid simulation using SPH due primarily to its simplicity. However, this scheme is not used in the current investigation.

c) Boundary Conditions

 Copyright © 2021 by National Research Council Canada

In DualSPHysics, the boundary is described by a set of particles that are considered as a separate set to the fluid particles. The software currently provides functionality for solid impermeable and periodic open boundaries. Methods to allow boundary particles to be moved according to fixed forcing functions are also available.

The Dynamic Boundary Condition (DBC) is the default method provided by DualSPHysics [Crespo et al., 2015] [22] to solid model boundaries. This method sees boundary particles that satisfy the same equations as fluid particles; however, their positions and velocities are not updated. Instead, they remain either fixed in position or move according to an imposed/assigned motion function (i.e. moving objects such as gates, wave-makers or floating objects). Using this boundary condition, when a fluid particle approaches a boundary particle, and the distance between them decreases beyond the kernel range, the density of the boundary particles increases, and giving rise to an increase in pressure. This results in a repulsive force being exerted on the fluid particle due to the pressure term in the momentum equation. This approach is not based on a rigorous physical derivation and is known to suffer from accuracy issues.

Nevertheless, this approach is easy to implement, computationally efficient, and naturally handles general 3-D shapes without any geometric boundary information. This method's stability relies on the length of time step taken being suitably short to handle the highest present velocity of any fluid particles currently interacting with boundary particles. Therefore, it is an important point when considering how the variable time step is calculated. All the SPH simulations carried out in this work used this boundary condition to define the boundaries of the structure and the numerical tank.

Within DualSPHysics, it is possible to define a pre-imposed movement for a set of boundary particles. Various predefined movement functions are available, and the ability to assign a time-dependent input file containing kinematic detail. These boundary particles behave as a DBC described above; however, they move independently of the forces currently acting upon them rather than fixed. This provides the ability to define complex simulation scenarios (i.e. a wave-making paddle) as the boundaries influence the fluid particles appropriately as they move.

d) Wave Modeling and Simulations

Piston-type long-crested wave generation schemes with second-order correction for long bound waves (sub-harmonics) available in DualSPHysics generate both monochromatic (regular) and random waves. The numerical flume resembles a physical wave facility so that the moving boundaries mimic the action of a piston-type wavemaker [15].

A passive wave absorption technique available in DualSPHysics is used for generating a long time series of waves in relatively short domains with negligible wave reflection. Passive wave absorbers are usually required to damp the wave energy and reduce reflection exerted by the model domain's boundary. A damping system is defined as a solution for passive absorption and is used to prevent wave reflection from fixed boundaries in the numerical flume [15]. The implemented absorption/damping system consists of gradually reducing the particles' velocity at each time step according to their location but using quadratic decay rather than exponential. This approach does not require a large region for wave absorption; a length up to 1 wavelength is generally recommended.

B. Finite Volume Method (FVM)

In this study, a commercial general-purpose CFD software, Star-CCM+, was used, which offers solutions for various representations of the Navier-Stokes equations. In the present research, the FVM based modelling of wave-structure interaction was carried out using Reynolds-averaged Navier-Stokes (RANS) equations with a realizable k-ε two-layer turbulence model. In addition, the free surface was modelled using the Volume of Fluid (VOF) method, and a High-Resolution Interface Capturing (HRIC) scheme was activated. Detailed formulation and equations of the applied numerical schemes can be found in the Star-CCM+ user manual.

C. Finite Difference Method (FDM) Model

The finite-difference numerical model (FDM) used here is formulated by vertical integration of the continuity equation and equations of motions in the x and y directions. The basic equations are as follows:

$$\eta_t + M_x + N_y = 0 \tag{7}$$

$$\begin{aligned} &M_t + (M^2/D)_x + (MN/D)_y + gD\eta_x + \varepsilon M \\ &+\frac{f_d}{2D^2} M\sqrt{M^2+N^2} = \mu\left(M_{xx} + M_{yy}\right) \\ &+(B+1/3)h^2\left(M_{xxt} + N_{xyt}\right) + Bgh^3\left(\eta_{xxx} + \eta_{xyy}\right) \\ &+hh_x\left(\frac{1}{3}M_{xt} + \frac{1}{6}N_{yt}\right) + \frac{1}{6}hh_yN_{yt} \\ &+Bgh^2\left[h_x\left(2\eta_{xx} + \eta_{yy}\right) + h_y\eta_{xy}\right] \end{aligned} \tag{8}$$

$$\begin{aligned} &N_t + (MN/D)_x + (N^2/D)_y + gD\eta_y + \varepsilon N \\ &+\frac{f_d}{2D^2} N\sqrt{M^2+N^2} = \mu\left(N_{xx} + N_{yy}\right) \\ &+(B+1/3)h^2\left(N_{yyt} + M_{xyt}\right) + Bgh^3\left(\eta_{yyy} + \eta_{xxy}\right) \\ &+hh_y\left(\frac{1}{3}N_{yt} + \frac{1}{6}M_{xt}\right) + \frac{1}{6}hh_xM_{yt} \\ &+Bgh^2\left[h_y\left(2\eta_{yy} + \eta_{xx}\right) + h_x\eta_{xy}\right] \end{aligned} \tag{9}$$

where η is the free surface at any given time, t the time, u and v the velocities in the x and y directions, $M = \int_{-h}^{\eta} u dz$ the mass flux in the x-direction, $N = \int_{-h}^{\eta} v dz$ the mass flux in the y-direction, g the gravitational acceleration, h the still water depth at any location, $D = h+\eta$ the instantaneous water depth at any location in the domain, μ the eddy viscosity defines the momentum exchange due to turbulence, B is an important factor in the dispersion relation that reduces the computational errors in the wave celerity, and group velocity and f_d is the energy dissipation coefficient used for the energy damping expression. A wave absorbing layer is a numerical energy-dumping zone in the model. An ADI (Alternating Directional Implicit) method is deployed for the solution of the above system of equations ([5], [1]).

Copyright © 2021 by National Research Council Canada

IV. MODELLING AND VALIDATION

A. SPH Numerical Wave Tank

In the present SPH-based investigation, the Numerical Wave Tank (NWT) was modelled by performing wave generation using piston-type second-order wave generation techniques [31] and the wave absorption/damping by a passive absorption technique. The second-order wave was created by correcting the first-order wave generation at the wavemaker by compensating both parasitic long waves and displacement long waves. The method implemented in DualSPHysics is based on the solution for the wavemaker's control signal that is described in [32]. The length of the wave absorption zone was close to one wavelength. In the NWT, the wave was generated immediately after the piston. However, the target wave was generated at approximately 25 m downstream of the wavemaker. The waves for the validation cases were completed both in deep and shallow water conditions. The layout of the numerical wave tank with wave damping zone is presented in Fig. 2.

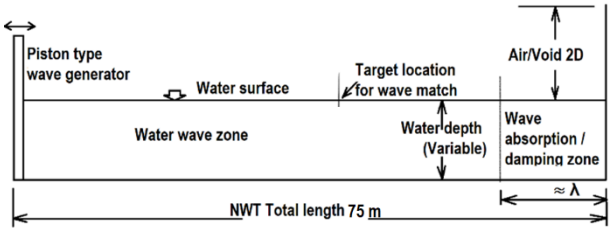

Fig. 2. Definition sketch of the NWT for modelling of free surface waves.

B. FVM Numerical Wave Tank

The NWT modelled in Star-CCM+ was as long as 9 wavelengths but very narrow for pseudo-2D application with symmetry conditions on sidewalls. The water depth was varying to match the test condition. Also, the wave damping zone was created on the outlet pressure with 2 wavelengths. The wave damping coefficient was adjusted as following Peric's suggestion [33]. A schematic of the FVM model domain is presented in Fig. 3.

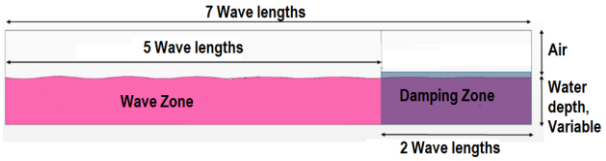

Fig. 3. Schematic representation of numerical domain for FVM based approach

For incident waves, the 5th order Stokes wave model was applied to consider the water depth effect properly. Five prismatic layers were attached to the structure and bottom. A fine mesh was generated around the free surface area based on 0.3% of wavelength and 3% of wave height, see Fig. 4.

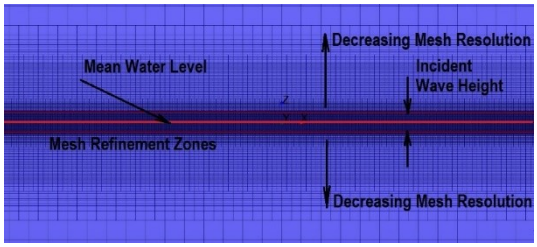

Fig. 4. Typical grids for FVM based approach.

C. FDM Numerical Wave Tank

The computational domain was 90m long and 80m wide.

Fig. 5 Computational domain for FDM (not to the scale)

In all three models, several numerical probes were utilized along the centerline of the domain for data acquisitions.

D. Simulation Cases

Free surface waves, both regular and irregular types and both shallow and deep water waves were investigated numerically in the present study. The axis of the models was parallel to the wave crests. The definition sketch of free surface waves is shown in Fig. 5. Deep and shallow water waves were investigated in the present study. Table 2 shows the incident wave properties used in this work. Here H (= $2a$, a is the amplitude) is the wave height and T is the period for regular waves, H_s is the significant wave height, and T_s is the significant wave period for irregular waves.

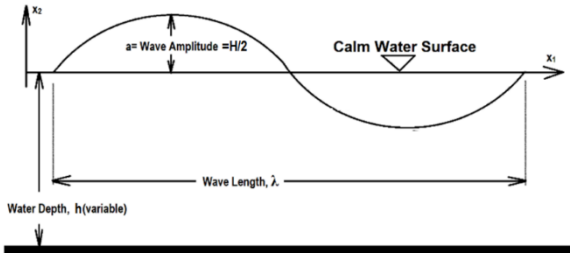

Fig. 5. Definition sketch of the free surface waves.

TABLE 2: SIMULATION CASES FOR THE WAVE VALIDATIONS AND COMPARISON STUDY.

ID	Water Depth (h, m)	Height, H/Hs (m)	Period T/Ts (s)	Wave Type	Wave Shape	SPH	FVM	FDM
1	0.505	0.10	1.11	Inter	Regular	X	X	X
2	0.505	0.10	1.67	Inter-Shallow	Regular	X	X	X
3	0.505	0.10	3.33	Shallow	Regular	X		X
4	0.505	0.10	1.42	Inter-Shallow	Irregular	X		X
5	2.8	0.49	3.00	Inter	Irregular	X		X

The current weakly compressible SPH computations are executed up to t=60s from the beginning for the regular waves and up to t=360s for the irregular waves, and it costs about 66 and 160 hours of CPU time using a personal computer (CPU 2.66 GHz and RAM 128.0 GMB with GPU capability). The

Copyright © 2021 by National Research Council Canada

FVM and FDM calculations were also carried out using the same PC.

E. SPH Convergence Study

The SPH NWT was used to perform a wave profile convergence study for the regular wave with ID 2. This case is chosen for the particle size or inter-particle distance and the smoothing length refinement study because this is a transitional wave. Table 3 and Fig. 6 summarized the results of the particle size convergence study and comparison with the corresponding OEB measurements in terms of wave height and period. Fig. 6 shows the particle size refinement study in terms of surface elevation, which was recorded at the wave measurement location (25 m downstream of the wave piston, approximately 3 times the wavelength. Based on the results, the inter-particle distance of 0.005 m was deemed sufficient and used for the remainder of the simulations.

TABLE 3: PARTICLE RESOLUTION CONVERGENCE STUDY FOR THE TARGET WAVE HEIGHT OF 0.1 M (6 M FULL SCALE) AND PERIOD OF 1.674 SEC (12.91 SEC. FULL SCALE).

Particle Size	Total Particles	Period	% Diff.	Height	% Diff.
[m]	*[M]*	*[sec.]*	*[-]*	*[m]*	*[-]*
0.01	0.38	1.674	-0.43	0.096	3.583
0.00875	0.53	1.671	-0.24	0.098	1.534
0.0075	0.68	1.671	-0.24	0.099	1.170
0.005	1.48	1.672	-0.33	0.100	-0.254
0.0375	2.65	1.674	-0.43	0.101	-0.515

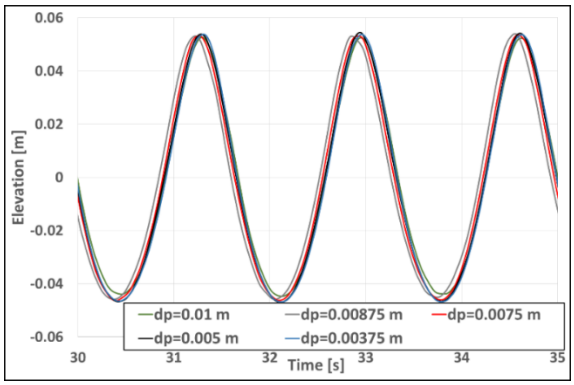

Fig. 6. Particle resolution convergence of SPH predicted water surface elevation for the target wave height of 0.1 m (6 m full scale) and period of 1.674 sec (12.91 sec. full scale).

Table 4 and Fig. 7 summarized the smoothing length convergence study results and comparison with the target wave height and period. Particle size of 0.0075m was used for all of these simulations. Fig. 7 shows the smoothing length refinement study in terms of surface elevation. Based on the results, the smoothing length parameter value of 1.75 was deemed sufficient and used for the remainder of the simulations.

TABLE 4: SMOOTHING LENGTH CONVERGENCE STUDY FOR THE MODEL VALIDATION FOR THE TARGET WAVE HEIGHT OF 0.1 M (6 M FULL SCALE) AND PERIOD OF 1.674 SEC (12.91 SEC. FULL SCALE).

Smoothing Length	Period	% Diff.	Height	% Diff.
[-]	*[sec.]*	*[-]*	*[m]*	*[-]*
1	1.669	-0.43	0.067	33.2
1.25	1.669	-0.24	0.082	17. 9
1.5	1.671	-0.24	0.097	3.1
1.75	1.671	-0.33	0.099	1.2
2	1.671	-0.43	0.099	1.03

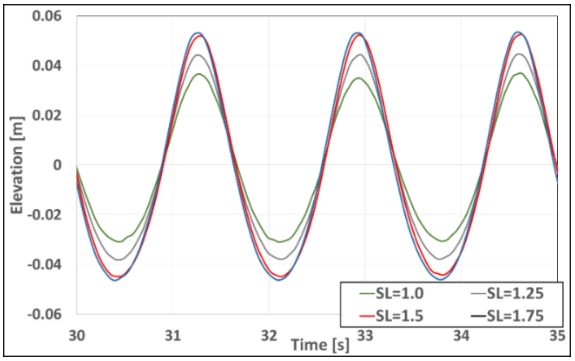

Fig. 7. Smoothing length convergence of SPH predicted water surface elevation for the target wave height of 0.1 m (6 m full scale) and period of 1.674 sec (12.91 sec. full scale).

F. FVM Convergence Study

A brief grid dependency study was carried out for the FVM model in Star-CCM+ for the ID 2 case. The base mesh size wave varied between 0.2 mm to 0.05 mm, and 0.1 mm was judged as sufficient for the simulations. Time step size was set to 0.5% of the wave period. However, the applied time step and the grid size may not be sufficient to capture the wave profile for very shallow water waves, but it is expected to be small enough to simulate the wave elevation for transitional and deep water waves.

For any numerical analysis, the performance of the numerical computation and the accuracy of data can be improved by many factors like the method itself, boundary conditions, grid/particle size, time interval, turbulence model, damping parameters, etc. In this FVM-based analysis, only grid size and time interval are taken care of for improvement, which can be modified by the researcher in the numerical computation analysis. We have not investigated the effect of the turbulence models, boundary conditions, damping factors, which should be investigated thoroughly.

V. RESULTS AND DISCUSSIONS

This paper presents a suite of metrics and methodologies, considering three key performance parameters: accuracy, computational requirements and available features for providing a consistent framework for the quantitative assessment of different techniques. Numerically simulated free surface elevations, wave periods, and spectrum (applicable to irregular waves) are compared with experimental data previously acquired at the Offshore Engineering Basin (OEB) of the NRC-OCRE. The accuracy of the numerical models in terms of deviations from target wave parameters and the basin measurements are presented. A brief discussion on the computational requirements and available features is presented; however, a detailed quantitative analysis is not presented. The results and discussions are presented for the deep water and shallow water waves separately. Both regular and irregular waves are discussed for both water depth conditions.

Copyright © 2021 by National Research Council Canada

A. *Deep Water Regular Waves*

Fig. 8 and Fig. 9 present a comparison of basin measurements and numerical predictions for wave elevation and periods for wave IDs 1 and 2, respectively. The predictions are obtained from the SPH, FDM and FVM –based tools. The results are presented in the basin (model) scale. Fig. 10, and Fig. 11 present the SPH and FVM predicted surface elevation for the entire simulation domain with a selected window zoomed in. Table 5 compares the average wave height and periods of the two regular waves between the predicted and the target waves. All three models are found to reproduce waves with an accuracy comparable to physical wave makers in the wave basin experiments for the regular deep-water waves; however, the SPH model provided the most accurate wave in terms of height and period and in terms of wave profile.

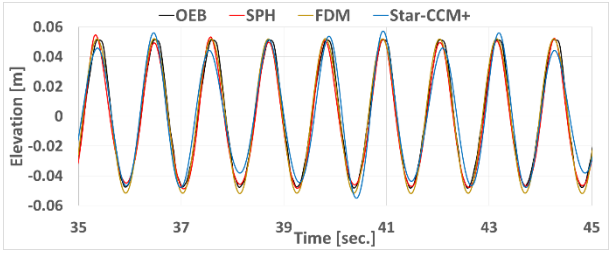

Fig. 8. Wave ID 1, Predicted by SPH, FDM and FVM, Compared with OEB Measurements; Model Scale h=0.505m, H=0.1m, T=1.112 sec.

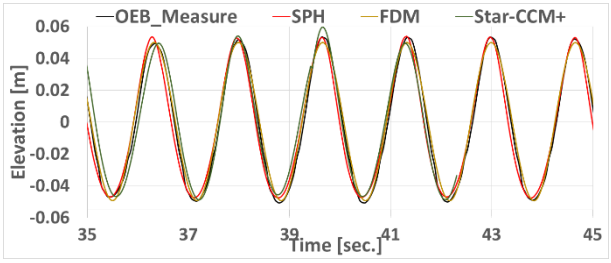

Fig. 9. Wave ID 2, Predicted by SPH, FDM and FVM, Compared with OEB Measurements; Model Scale h=0.505 m, H=0.1 m, T=1.667 sec.

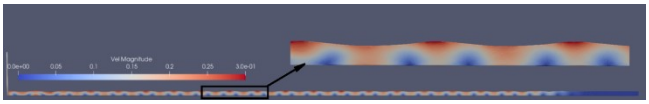

Fig. 10. The SPH Predicted Wave Elevation; Model Scale h=0.505 m, H=0.1 m, T=1.667 sec.

Fig. 11. The FVM Predicted Wave Elevation; Model Scale h=0.505 m, H=0.1 m, T=1.667 sec.

TABLE 5: COMPARISON OF WAVE HEIGHT AND PERIOD OF THE MEASURED AND PREDICTED REGULAR WAVES WITH THE TARGET WAVES; MODEL SCALE H=0.505 M, H=0.1 M, T=1.667 SEC.

	Height (m)	% Diff	Period (sec.)	% Diff
Wave ID 01, H=0.1 m, T=1.11 sec.				
OEB	0.1078	-7.8	1.11	0.1
SPH	0.0973	2.7	1.11	-0.3
FDM	0.0981	1.9	1.13	-1.8
Star-CCM+	0.0982	1.8	1.12	-0.8
Wave ID 02, H=0.1 m, T=1.667 sec.				
OEB	0.1028	-2.8	1.67	0.1
SPH	0.1003	-0.3	1.67	-0.2
FDM	0.0992	0.8	1.67	-0.1
Star-CCM+	0.1055	-5.5	1.60	3.8

B. *Deep Water Irregular Waves*

Fig. 12 and Fig. 13 present a comparison of basin measurements and numerical predictions for wave elevation time series and wave power spectral density for the transitional water extreme wave with ID 4, respectively. Table 6 present a quantitative comparison of the total spectral energy, significant wave height and modal wave periods of the extreme irregular wave between the predicted and the target waves. Both SPH and FDM models reproduced waves with an accuracy comparable to physical wave makers in the wave basin experiments for the deep-water regular waves; however, the SPH model provided the most accurate wave in terms of height and period well as in terms of wave profile. Note that the basin wave was generated based on a Torsethaugen spectrum, hence the deviation of the spectrum profile from the predicted ones.

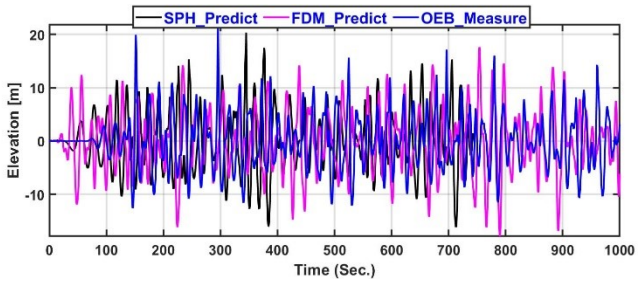

Fig. 12. The measured and predicted time series of the transitional water irregular wave.

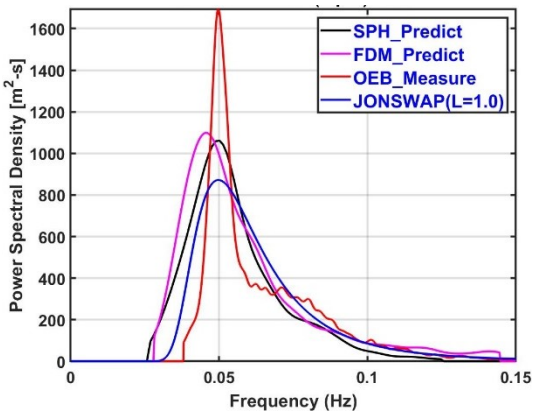

Fig. 13. The Comparison of Power Spectrum between the Measured and Predicted Transitional Water Irregular Extreme Wave.

TABLE 6: COMPARISON OF SPECTRUM ENERGY (M0), SIGNIFICANT WAVE HEIGHT (HS) AND MODAL PERIOD (TP) OF THE MEASURED AND PREDICTED TRANSITIONAL EXTREME IRREGULAR WAVES WITH THE TARGET WAVES.

	SPH	FDM	OEB	Ideal
m0	31.62	36.47	27.93	30.27
Hs	22.49	24.15	21.14	22.00
Tp	20.20	21.78	20.00	20.05

Copyright © 2021 by National Research Council Canada

C. Shallow Water Regular Waves

Fig. 14 compares the basin measurements and numerical predictions for wave elevation and periods for the extremely shallow water wave with ID 3. The predictions are obtained from the SPH and FDM models; however, the FVM –based tools could not produce the desired results, hence not presented. The results are presented in the basin (model) scale. Fig. 15 presents the SPH predicted surface elevation for the entire simulation domain with a selected window zoomed in. Table 5 present a quantitative comparison of the average wave height ad periods of the two regular waves between the predicted and the target waves. Table 6 presents a quantitative comparison of the average wave height and shallow water regular wave periods between the predicted and the target waves. Both SPH and FVM models reproduce waves accurately comparable to physical wave makers in the wave basin experiments for both the deep and shallow water waves; however, the SPH model provided the most accurate wave in terms of height and period well as in terms of wave profile. The basin floor distorts the wave trough for extremely shallow water. This effect was well-captured by the SPH model.

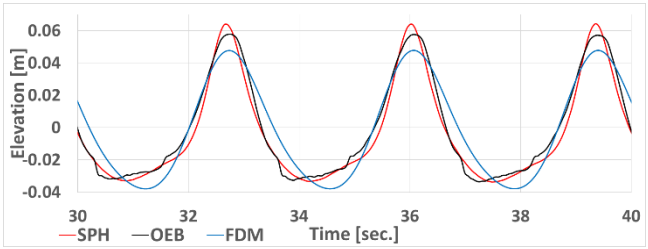

Fig. 14. Wave ID 3, Predicted by SPH, and FDM, Compared with OEB Measurements; Model Scale h=0.505m, H=0.1m, T=3.334 sec.

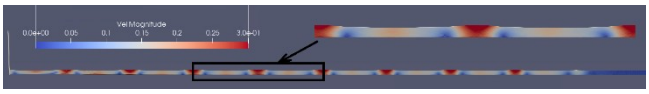

Fig. 15. The wave profile of wave ID 3, Predicted by SPH; Model Scale h=0.505 m, H=0.1 m, T=3.333 sec.

TABLE 7: COMPARISON OF WAVE HEIGHT AND PERIOD OF THE MEASURED AND PREDICTED SHALLOW WATER REGULAR WAVES WITH THE TARGET WAVES; MODEL SCALE H=0.505 M, H=0.1 M, T=3.334 SEC.

	Height (m)	% Diff	Period (sec.)	% Diff
OEB	0.093	6.6	3.33	0.0
SPH	0.097	3.1	3.35	-0.4
FDM	0.086	14.4	3.33	0.0

D. Shallow Water Irregular Waves

Fig. 16, Fig. 17, Fig. 18 compare the basin measurements and numerical predictions for wave elevation time series and wave power spectral density for the shallow water extreme wave with ID 5, respectively. Table 8 present a quantitative comparison of the total spectral energy, significant wave height and modal wave periods of the extreme irregular wave between the predicted and the target waves. Both SPH and FDM models are found to reasonably reproduce waves with an acceptable accuracy comparable to physical wave makers in the wave basin experiments for the shallow regular waves; however, the SPH model provided the most accurate wave in terms of height and period as well as in terms of wave profile. Note that the basin wave was generated based on a JONSWAP spectrum with a peakedness of γ=2.0; the SPH and FDM predicted spectrum profile is well matched to that of the measurements.

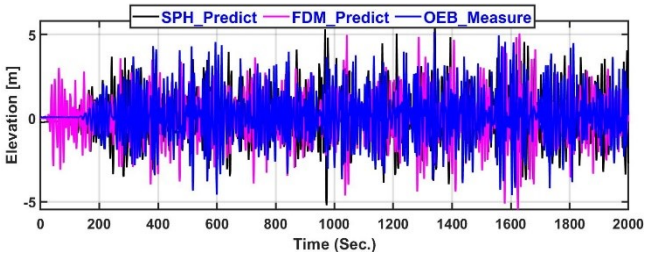

Fig. 16. The measured and predicted time series of the shallow water irregular wave.

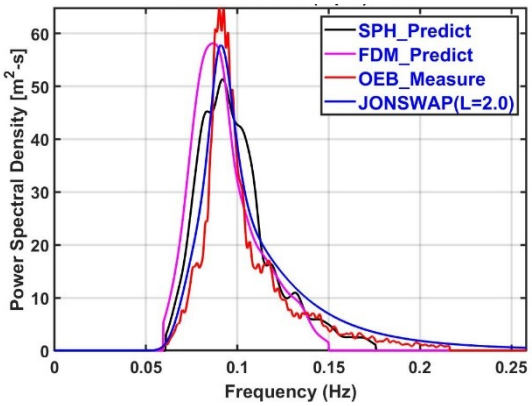

Fig. 17. The Comparison of Power Spectrum between the Measured and Predicted Shallow Water Irregular Wave.

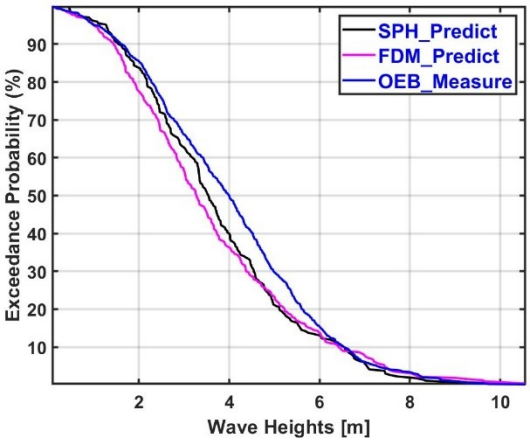

Fig. 18. Comparisons of the probability of exceedance (PoE) of wave heights between the Measured and Predicted Shallow Water Irregular Wave.

TABLE 8: COMPARISON OF SPECTRUM ENERGY (M0), SIGNIFICANT WAVE HEIGHT (HS) AND MODAL PERIOD (TP) OF THE MEASURED AND PREDICTED SHALLOW WATER IRREGULAR WAVES WITH THE TARGET WAVES.

	SPH	FDM	OEB	Ideal
m0	2.19	2.23	1.83	2.25
Hs	5.92	5.97	5.42	6.00
Tp	10.86	11.52	11.10	11.00

Table 9 presents a comparison of the computational time between the three modelling approaches. Although it was observed that the SPH model revealed better results than the other two models for the limited waves considered here, the

Copyright © 2021 by National Research Council Canada

computational time was significantly larger in SPH simulations compare to the other two models, particularly the FDM model. Table 10 presents a preliminary comparison of the available wave modelling features between the three models. The comparison is subjective and should be considered tentative.

TABLE 9: COMPARISON OF COMPUTATIONAL TIME BETWEEN THE THREE MODELLING APPROACHES.

ID	Regular / Irregular	SPH	FDM	FVM
1	Regular	28 hrs (60 sec.)	0.5 hrs (60 sec.)	12 hrs (15 sec.)
2	Regular	28 hrs (60 sec.)	0.5 hrs (60 sec.)	12 hrs (15 sec.)
3	Regular	28 hrs (60 sec.)	0.5 hrs (60 sec.)	
4	JONSWAP	55 hrs (360 sec.)	2.5 hrs (360 sec.)	
5	P-M	96 hrs (360 sec.)	2.5 hrs (360 sec.)	

TABLE 10: COMPARISON OF AVAILABLE FEATURES BETWEEN THE THREE MODELLING APPROACHES.

	Features	SPH	FVM	FDM
1	Model setup	Easy and flexible	Difficult and time-consuming	Simple and Quick
2	Shallow water modelling	Excellent	Developing	Very well
3	Irregular wave modelling	Excellent	Developing	Very well
4	Turbulence modelling	Developing	Excellent	Not done yet
5	Breaking waves	Excellent	Challenging	Very well

Regarding the three assessment criteria, significant differences were found between the three methods, and no single method performed best in all aspects of the assessment across the different test cases. The deterministic comparisons between the basin measurements and numerical predictions revealed the deficiencies in both facilities. The challenge remains for wave basins to reduce unwanted basin effects and numerical facilities to accurately model waves properly account for boundary effects and numerical diffusions. In addition, only flat-bottom domains were considered in the investigation, leaving the wave modelling for uneven bottom for future studies.

CONCLUSIONS

The prediction performance of three numerical techniques, namely an open-sourced smoothed particle hydrodynamics (SPH) code, a finite difference method (FDM) based a 3D dispersive numerical model with enhanced dispersion characteristics, and a commercial CFD code (Star CCM+), has been investigated by comparing their accuracy relative to corresponding basin measurements and target parameters for huge regular and irregular waves of different steepness in both deep water and shallow water conditions.

Numerically simulated free surface elevations, wave periods, and spectrum (for irregular waves only) are compared with experimental data. All three models reproduced waves with an accuracy comparable to physical wave makers in the wave basin experiments for the deep-water regular and irregular waves. It was observed that the SPH model revealed better results than the other two models for the limited shallow-water waves considered here, although the computational time was significantly larger in SPH simulations compare to the FDM model. All simulations carried out by SPH, and FVM methods were completed in 2D; the FDM simulations were carried out in full 3D.

The challenge remains for wave basins to reduce unwanted basin effects and numerical facilities to accurately model waves with proper account for boundary effects and numerical diffusions. In addition, only flat-bottom domains were considered in the investigation, leaving the wave modelling for uneven bottom for future studies.

Future studies should include investigating the effect of various influential factors such as the turbulence models, boundary conditions, damping coefficients, etc., to obtain more accurate results from the FVM predictions.

The current study should be extended to predict the waves for an extended period to ensure minimum numerical diffusions and loss of energy and minimum wave reflections. The FVM often fails to predict waves without decays for an extended period. The effect of bottom friction and shape on the wave profile and other characteristics should be investigated. The capabilities of the SPH and FVM models for the spatial distribution of the wave should also be investigated.

ACKNOWLEDGMENT

All personnel, who have contributed to this project in any form, deserve our sincere gratitude. The authors are indebted to the National Research Council's Ocean Coastal and River Engineering Research Center for supporting this numerical modelling endeavour.

REFERENCES

[1] T. Hiraishi, I. Uehara and Y. Suzuki, "Applicability of wave transformation model in Boussinesq equations," Report of the Port and Harbor Research Institute, Japan, No.814, pp.1-22, 1995.

[2] P.A. Madsen and O.R. Sørensen, "A new form of Boussinesq equations with improved linear dispersion characteristics, Part 2. A slowly varying bathymetry," Coastal Engineering, Elsevier, 18, pp.183-204, 1992.

[3] G. H. Peregrine, "Long wave on a beach," JFM, Vol:27, Part:4, pp.715-827, 1967.

[4] M. H. Zaman, T. Hiroyoshi and R. E. Baddour, "Propagation of monochromatic water wave trains," Ocean Engineering, Elsevier, 34, pp.1850-1862, 2007.

[5] M. H. Zaman, K. Hirayama and T. Hiraishi, "An extended Boussinesq model and its application to long period waves," Proc. 11th ISOPE Conf., 3, pp.607-614, 2001.

[6] D. Violeau and B.D. Rogers, "Smoothed particle hydrodynamics (SPH) for free-surface flows: past, present and future," Journals of Hydraulic Research. 54 (1), 1–26, 2016.

[7] F. Aristodemo, G. Tripepi, D-D. Meringolo and P. Veltri, "Solitary wave-induced forces on horizontal circular cylinders: Laboratory experiments and SPH simulations," Coastal Engineering, Volume 129, pp 17-35, 2017. ISSN 0378-3839, https://doi.org/10.1016/j.coastaleng.2017.08.011.

[8] L. Delorme, A. Colagrossi, A. Souto-Iglesias, R. Zamora-Rodríguez and E. Botía-Vera, « A set of canonical problems in sloshing, Part I: pressure field in forced roll comparison between experimental results and SPH," Ocean. Eng. 36 (2), pp 168–178, 2009

[9] P. Sun, F. Ming and A. Zhang, "Numerical simulation of interactions between the free surface and rigid body using a robust SPH method," Ocean. Eng. 98, pp 32–49, 2015.

[10] E. Pugliese Carratelli, G. Viccione and V. Bovolin,"Free surface flow impact on a vertical wall: a numerical assessment," Theor. Comp. Fluid Dyn. 30 (5), pp 403–414, 2016.

 Copyright © 2021 by National Research Council Canada

[11] F Aristodemo, I. Federico, P. Veltri and A. Panizzo, "Two-phase SPH modelling of advective-diffusion processes," Environ. Fluid Mech. 10, pp 451–470, 2010.

[12] I. Federico, S. Marrone, A. Colagrossi, F. Aristodemo and M. Antuono, "Simulating 2D open-channel flows through an SPH model," Eur. J. Mech. B/Fluids 34, pp 35–46, 2012.

[13] F. Aristodemo, S. Marrone and I. Federico, "SPH modelling of plane jets into water bodies through an inflow/outflow algorithm," Ocean. Eng. 105, pp 160–175, 2015.

[14] R. Dalrymple and B. Rogers, "Numerical modelling of water waves with SPH method," Coastal Engineering, Vol 53, No 2-3, pp 141-147, 2006.

[15] C. Altomare, J.M. Domínguez, A.J.C Crespo, J. Gonz_alez-Cao and T. Suzuki, "Long-crested wave generation and absorption for SPH-based DualSPHysics model," Coastal Engineering 127, pp 37–54, 2017.

[16] C. Altomare, A.J.C Crespo, J. M. Domínguez, M. G_omez-Gesteira, T. Suzuki and T. Verwaest,"Applicability of Smoothed Particle Hydrodynamics for estimation of sea wave impact on coastal structures," Coast. Eng. 96, pp 1–12, 2015.

[17] D.D. Meringolo, F. Aristodemo and P. Veltri, P, "SPH numerical modelling of wave perforated breakwater interaction," Coast. Eng. 101, pp 48–68, 2015.

[18] B. Ren, H. Wen, P. Dong and Y. Wang, Y, " Numerical simulation of wave interaction with porous structures using an improved smoothed particle hydrodynamic method," Coast. Eng. 88, pp 88–100, 2014.

[19] B. Bouscasse, A. Colagrossi, S. Marrone and M. Antuono, "Nonlinear water wave interaction with floating bodies in SPH," J. Fluids Struct. 42, pp 112–129, 2015.

[20] A. Barreiro, A.J.C. Crespo, J. M. Domínguez, O. García-Feal, I. Zabala, M. G_omez-Gesteira,." Quasi-Static Mooring solver implemented in SPH," J. Ocean Eng. Mar. Energy 2 (3), pp 381–396, 2016.

[21] Crespo, A.J.C., Altomare, C., Domínguez, J.M., Gonz_alez-Cao, J., G_omez-Gesteira, M., 2017. Towards simulating floating offshore oscillating water column converters with Smoothed Particle Hydrodynamics. Coast. Eng. 126, 11–26.

[22] Crespo, A.J.C.; Domínguez, J.M.; Rogers, B.D.; Gómez-Gesteira, M.; Longshaw, S.; Canelas, R.; García-Feal, O., 2015. DualSPHysics: Open-Source Parallel CFD Solver Based on Smoothed Particle Hydrodynamics (SPH). Comput. Phys. Commun. 2015, 187, 204–216.

[23] Wendland H. Piecewise polynomial, positive definite and compactly supported radial functions of minimal degree. Advance Computational Mathematics, 1995; 4: 389‑96. https://doi.org/10.1007/BF02123482.

[24] Monaghan JJ. 1994. Simulating free surface flows with SPH. Journal of Computational Physics, 110, 399–406.

[25] Monaghan JJ. Cas, RAF, Kos AM, Hallworth M, 1999. Gravity currents descending a ramp in a stratified tank. Journal of Fluid Mechanics, 379, 39–70.

[26] Mohaghan, J., 2012, Smoothed Particle Hydrodynamics and Its Diverse Applications, Annual Review of Fluid Mechanics, Vol 44, pp 323-346, 2012.

[27] Liu, M., Liu, G., 2010, Smoothed Particle Hydrodynamics (SPH): an Overview and Recent Developments", Archieves of Computational Methods in Engineering, Vol. 17, no.1, pp 25-76, 2010.

[28] Molteni, D., Colagrossi, A., 2009, A Simple procedure to improve the pressure evaluation in hydrodynamic context using the SPH, Computer Physics Communications, Vol 180, No. 6, 861-872, 2009.

[29] Lo, E. Y. M. and Shao, S. D., Simulation of near-shore solitary wave mechanics by an incompressible SPH method, Applied Ocean Research, 24(5), 2002, 275-286.

[30] Monaghan JJ. 1992. Smoothed particle hydrodynamics. Annual Review of Astronomy and Astrophysics, 30, 543- 574.

[31] Madsen, O. S., 1971. On the generation of long waves. J. Geophys. Res. 76, 8672–8673.

[32] Barthel FC, Mansard V, Sand P, Vis SE. 1983. Group bounded long waves in physical models. Ocean Engineering, 10, 261–294.

[33] Peric, R., and Moustafa, A-M. (2015). Reliable Damping of Free Surface Waves in Numerical Simulations. Ship Technology Research. 63. 10.1080/09377255.2015.1119921.

[34] Windt, C., Davidson, J., Schmitt, P., & Ringwood, J., 2019. On the Assessment of Numerical Wave Makers in CFD Simulations. Journal of Marine Science and Engineering, 7, 47.

[35] Windt, C., Davidson, J., Ringwood, J., , 2018. High-fidelity numerical modelling of ocean wave energy systems: A review of CFD-based numerical wave tanks. Renew. Sustain. Energy Rev. 2018, 93, 610–630.

[36] Wang, W., Kamath, A., Pákozdi, C., & Bihs, H. (2020). A Comparison of Different Wave Modelling Techniques in An Open-Source Hydrodynamic Framework. Journal of Marine Science and Engineering, 8, 526.

[37] Lamb, H., 1945. Hydrodynamics, sixth ed. Dover, New York, pp. 1–306.

[38] Stoker, J.J., 1957. Water Waves. Interscience, New York, pp. 1–567.

[39] Ursell, F., 1953. The long-wave paradox in the theory of gravity waves. Proceedings of the Cambridge Philosophy Society 49, 685–694.

[40] Peregrine, D.H., 1967. Long waves on a beach. Journal of Fluid Mechanics 27 (4), 815–827.

[41] Horikawa, K., 1988. Nearshore dynamics and coastal processes. University of Tokyo Press, pp. 1–522.

[42] Ohyama, T., Kioka, W., Tada, A., 1995. Applicability of numerical models to nonlinear dispersive waves. Coastal Engineering Elsevier Science Publication B. V. 24, 301–311.

[43] Phillips, O.M., 1997. The Dynamics of the Upper Ocean, second ed. University Press, Cambridge.

[44] Herbers, T.H.C., Burton, M.C., 1997. Nonlinear shoaling of directionally spread waves on a beach. Journal of Geophysical esearch 102 (C9), 21101–21114.

[45] Lara, J. L., Garcia, L. and Losada, I. J. RANS modelling applied to random wave interaction with submerged permeable structures. Coastal Engineering, Elsevier Science Publication B. V. 53, 395-417.

[46] Beji, S., Nadaoka, K., 2004. Fully dispersive nonlinear water wave model in curvilinear coordinates. Journal of Computational physics 198, 645–658.

[47] Madsen, P., Sorensen, O., 1993. Bound waves and triad interactions in shallow water. Ocean Engineering 18, 183–204.

[48] Kaihatu, J.M., Kirby, J.T., 1995. Nonlinear transformation of waves in finite water depth. Physics of Fluid 7 (8), 1903–1914.

 Copyright © 2021 by National Research Council Canada